IIETA International Information and Engineering Technology Association
Advancing the World of Information and Engineering

Traitement du Signal
Vol. 43, No. 1, February, 2026, pp. 233-247
Journal homepage: http://iieta.org/journals/ts

Automatic Diagnosis of Common Carotid Artery and Plaque Grading Using Novel Deep Learning Model

Preethi Siva[1*], Arunadevi Baladhandapani[1], Deepa Subramaniam Nachimuthu[2]

[1] Department of Electronics and Communication Engineering, Dr. N.G.P. Institute of Technology, Coimbatore 641048, India
[2] Department of Electrical Engineering, National Institute of Technology Calicut, Kozhikode 673601, India

Corresponding Author Email: preethi.s@drngpit.ac.in

https://doi.org/10.18280/ts.430117

Received: 31 January 2025
Revised: 25 August 2025
Accepted: 1 October 2025
Available online: 28 February 2026

Keywords:
Common Carotid Artery (CCA), deep learning, intima-media thickness measurement, support vector machine, ultrasound imaging, vision transformer

ABSTRACT

Accurate diagnosis of Common Carotid Artery (CCA) disease is crucial for preventing stroke and guiding appropriate treatment strategies. This study introduces a Computer-Aided Diagnosis System (CADS) to diagnose CCA disease and assess plaque severity from longitudinal ultrasound images. The introduced system integrates multiple processing stages to enhance diagnostic accuracy. Initially, Ultrasound (US) images undergo denoising using the Circular Median Filter (CMF) to remove noise. Modified Arithmetic Optimization Algorithm (AOA) is implemented to determine the finest threshold to isolate the CCA lumen from its history. The Intima Media Thickness (IMT) is estimated through aspect detection accompanied by morphological operations. The segmented region is classified using a Vision Transformer (ViT). The system performs plaque grading using Support Vector Machine (SVM) to quantify disease severity. Each technique inside the proposed system contributes uniquely to its functionality, distinguishing it from preceding research. The performance of the proposed CADS is validated on the CUBS dataset. Effectiveness of the model is evaluated by computing Peak Signal-to-Noise Ratio (PSNR), Jaccard Similarity Index (JSC), Dice Coefficient (DC), accuracy, specificity, sensitivity, Balanced Accuracy (BA), precision, Negative Predictive Value (NPV), and Matthew's Correlation Coefficient (MCC). The integration of advanced processing techniques, optimal thresholding, and ViT and SVM-based classification ensures accurate diagnosis and effective plaque grading. The proposed model attained an accuracy value of 92.63% for CCA detection and 86.32% for plaque grading. The proposed CADS not only enhances diagnostic accuracy but also aids in the quantitative assessment of plaque, supporting better patient outcomes and clinical decision-making. Comparative analysis against clinician-delineated results demonstrates the superiority of the introduced CADS in accuracy and reliability.

1. INTRODUCTION

The human body's cardiovascular system is a vital organ that keeps us alive. They are a component of the cardiovascular system and carry blood from the heart, and they ensure that every organ in the body functions properly. The primary components of these vessels are arteries and veins that facilitate blood flow throughout the body [1]. Any barrier in these vessels can significantly reduce organ function. Heart disease, or CVD is the major cause of mortality and disability. The accumulation of fat and cholesterol on the artery walls is a characteristic of this chronic degenerative disease [2]. Common Carotid Artery (CCA) disease, peripheral vascular disease, and coronary artery disease are the most prevalent CVDs. The main cause of CVD and stroke is atherosclerosis. Atherosclerosis is a condition that thickens and reduces the elasticity of the arterial walls, causing blood flow to the brain and head [3]. CCA is important for the blood supply in the frontal areas of the brain responsible for cognitive functions. The patient is at risk for stroke and heart disease because the CCA is narrowed [4]. Reducing mortality and expanding lifestyle depend on the initial atherosclerosis diagnosis and detection. Estimation of Intima-Media thickness (IMT) as a major indicator for initial identity.

A series of atherosclerosis diagnostic tests, such as imaging tests, cardiac catheterization, angiography, and blood tests, including C-Reactive Protein. The most popular method of diagnosis is imaging-based, as it indirectly enables visualization and classifies lesions. These imaging modalities include magnetic resonance imaging (MRI), ultrasound (US), and computed tomography (CT) [5, 6]. The US imaging represents one of the most promising imaging forms to determine the IMT and understand the properties of carotid arteries. There are benefits of real-time, non-invasive, reliable, inexpensive, radiation-free, and patient-safe US imaging. However, unlike US images, the resolution and signal-to-noise ratio are low. Additionally, speckle noise, which often results in blurred and worse image quality, is an intrinsic effect of these images [7]. The segmentation technique is complicated when speckle noise in carotid US images deteriorates the image quality. To address such an issue, researchers have used several techniques for preprocessing carotid US images like

Anisotropic diffusion filter, lee filter, non-local mean fitter, and lee filter. Competent sonographers usually estimate the IMT. When managing large image databases, this method is time-consuming, difficult, subjective, and dependent on the user. The sonographer must choose seed points for segmentation to do the IMT measurement using semi-automated measurements [8]. Compared to manual and semi-automated approaches, automation offers more benefits.

IMT assessment in carotid US images has been the focus of many methods in recent years, including Hough transform-based models, active contour models, multi-resolution edge-snapper methods, and combining the Bayesian model with dynamic and gradient programming [9, 10]. However, rather than resilience, these models prioritize IMT measurement precision. Functions and their derivatives are used in edge-based approaches. The function's inconsistencies cause it to perform poorly. Because non-gradient-based algorithms depend just on the function and not on the derivatives, they have been presented. The non-gradient approach, the thresholding technique, is used for IMT segmentation. Grayscale values are used in thresholding techniques to differentiate an item from its background. The objective function has been used to incorporate thresholding approaches to determine the optimum solution. Segmentation thresholding techniques include Tsallis entropy, Kapur's entropy, and Ostu's thresholding. Previous studies have proposed heuristic methods for segmentation, including Particle Swarm Optimization (PSO) [11], Ant Colony Optimization (ACO) [12], and Wind-Driven Optimization (WDO) [13]. However, these algorithms are hard to compute when utilized for multilayer thresholding. To solve this problem, we suggest using thresholding-based segmentation based on the Arithmetic Optimization Algorithm (AOA).

This research proposes a comprehensive Computer-Aided Diagnosis System (CADS) for the identification and categorization of plaque in carotid artery disease. The proposed system involves several phases, such as preprocessing, segmentation, IMT measurements, and two-level classification. Initially, a denoising filter, the Circular Median Filter (CMF), is applied to eliminate noise. Secondly, the modified Arithmetic Optimization Algorithm (AOA) is proposed to segment the Region of Interest (ROI) from its background. Thirdly, IMT is computed for the ROI. Fourthly, Vision Transformer (ViT) is used to classify images into two categories: normal and abnormal. Finally, to determine the illness severity, US images are classified using a Support Vector Machine (SVM). To demonstrate its validity, the acquired results are contrasted with clinical values and previous techniques. A summary of the paper's scientific contributions is provided below:

- A fully automated system is designed to diagnose carotid artery disease using a two-level classifier to attain optimal classification performance.
- A denoising filter, CMF is designed to suppress noise from the input images.
- A threshold-based segmentation utilizing Modified AOA is proposed to accurately extract ROI from the background.
- A first-level classifier using ViT is designed to classify CCA longitudinal images into normal or abnormal.
- A second-level classifier utilizing SVM is implemented to assess the grade of plaque in abnormal cases.
- Scalability and robustness of the proposed system are validated on the CUBS database to ensure generalizability.
- The efficacy of the suggested system is assessed using a number of tests and comparisons with benchmark models.
- A pioneering automated framework is presented for carotid artery disease diagnosis and plaque grading.
- To the author's knowledge, this work represents the first attempt to develop a completely automated method for diagnosing and rating plaque and carotid artery disease.

The following is an overview of the remaining portions of the paper: The literature is presented in Section 2, and the approach is explained in Section 3. Section 4 provides the results of numerical and environmental testing. Conclusion and future efforts are given in Section 5.

2. REVIEW OF LITERATURE

Several methods have been developed for CCA segmentation and diagnosis using different strategies. This section provides a review of recent works related to CCA segmentation and classification.

For tasks involving medical image analysis, including preprocessing, segmentation, and diagnosis, machine learning (ML) and deep learning (DL) algorithms have emerged as intriguing and promising approaches. DL based Intima-media Complex (IMC) segmentation was described by Mohammed et al. [1]. Four DL models, such as Convolutional Neural Network (CNN), transformer-based, pixel difference-based, and self-organizing operational neural networks, were employed for isolating IMC from the CUBS data. Results demonstrated that deep learning models can offer significant improvements in IMC segmentation. However, deep learning models require extensive data to achieve satisfactory results.

Menchón-Lara and Sancho-Gómez [3] presented an ML model for IMT division in American images. From his perspective, the US images were prepared to identify ROI. To each pixel, to produce an intensity pattern, a windowing approach to ROI was used. These intensity patterns were represented as a feature space using an autoencoder. An Artificial Neural Network (ANN) was used to identify Lumen Intima (Li) and Media Adventitia (MA) interfaces. However, this method's dependence on an autoencoder can cause information loss during a decrease in diarrhea, potentially affecting the division's accuracy.

Nagaraj et al. [7] used a Wind Driven Optimization (WDO) method to fragment IMT depending on a certain point. To remove noise, images were denoised using an Optimized Bayesian Non-Local Mean (OBNLM) filter. After this, total variation followed by morphological operations was employed to improve visual appearance and clean the borders and edges. A Canny edge detector was applied to detect edges. Finally, a threshold-based WDO algorithm was implemented to estimate IMT. This method may not generalize well across different US systems.

Rocha et al. [14] showed a way to divide US images into near-end and far-end intima regions. The authors were able to make accurate predictions for IMT by using geometric snakes, dynamic programming, and smooth intensity thresholding. Geometric snakes may use a significant amount of processing power and be sensitive to where the beginning contour is positioned. This might cause problems when the intima layers are not perfectly constructed.

Naik et al. [15] provided a thorough analysis of methods available for carotid artery segmentation in US images, along with their merits and weaknesses. A data mining model for plaque grading was introduced by Molinari et al. [16]. US

images were preprocessed using CLATHE and then decomposed using the Bidirectional Empirical mode decomposition method. Energy features were computed, and then the dimension of features was reduced using some tests, such as the t-test and the Wilcoxon test. Finally, Linear Discriminant Analysis (LDA) was adopted to differentiate between plaque that is asymptomatic and that is symptomatic. This method may suffer from computational inefficiency due to feature decomposition and preprocessing steps.

Latha et al. [17] recommended an automatic segmentation method for carotid Artery segmentation. US images were denoised with the curvelet transform with the soft thresholding technique. Affinity Propagation followed by Density-Based Spatial Clustering of Applications with Noise (AB+DBSCAN) was adopted for segmentation. Results were compared with the PSO and IDO algorithms. Clustering methods like AB+DBSCAN may struggle with noise and artifacts, leading to inconsistent segmentation results.

Vila et al. [18] suggested a method based on DenseNet for plaque segmentation and IMT estimation. This method does not need any ROI extraction. Input images were applied to a densely connected CNN for semantic segmentation. After segmentation, IMT is estimated, and plaque is detected. Deep learning-based models are resource-intensive, requiring substantial computational power. Huang et al. [19] provided a comprehensive survey of CCA disease diagnosis methods using DL, along with their merits and drawbacks.

He et al. [20] designed a Bilinear CNN with a residual Neural network (BCNN-Resnet) to recognize carotid plaques. To eliminate unnecessary background, input images were cropped to a uniform size. Flipping, scaling, and rotation were some of the augmentation methods employed to expand the database's ability. BCNN-ResNet was applied to perform classification task. Resizing images could potentially distort anatomical structures, impacting segmentation accuracy.

Kumar et al. [21] used active oblongs to segment CCA images. But an active oblongs-based segmentation method may struggle with anatomical variations and irregularities. Jain et al. [22] developed an automated system using DL and reported satisfactory results. Özdemir et al. [23] explored an ML model for carotid artery disease diagnosis. High classification accuracy was attained by the technique using a super learning model that combines random forest, gradient boosting, and adaptive boosting. Although this method increased the size of the dataset to 1000 by means of an augmentation method. The original images were 122, relatively small. This may limit the generalizability of the model.

CCA disease is a serious global medical problem, and prevention depends on early disease recognition. Fitas and Goncalves [24] investigated how to enhance data for the detection of carotid artery disease using Generative Adversarial Networks (GAN). Both original and enhanced data were used to confirm the classification rate of four deep learning models: AlexNet, VGGNet, GoogleNET, and CifarNet. Results highlighted the power of GAN in improving deep learning models for medical image analysis. Nevertheless, training a GAN is computationally intensive and can be challenging to stabilize, requiring significant computational resources.

Koloi et al. [25] predicted early-stage coronary artery disease using a machine learning model. The authors considered 331 original images and then applied some techniques to generate high-quality virtual data to improve the machine learning model performance. Gradient boosting showed better performance than random forest in terms of accuracy. Ottakath et al. [26] presented a Bi-attention doubleUNet for carotid artery segmentation. This approach combined channel-wise and spatial attention with a bottleneck module. The model was tested on US images and reported superior segmentation performance. The drawback of the method is that the effectiveness relies on high-quality US images.

2.1 Research issue and contributions

This paper presents significant advancements in the development of the CADS for carotid artery disease. The system is distinct in implementing a five-phase process, which sets it apart from previous methods in this domain. The primary contributions of this work are outlined across several key dimensions:

First, this research presents a novel CADS system that incorporates a series of sophisticated processes not previously combined in this manner. Each phase contributes to the overall innovation:

Preprocessing: A new CMF is proposed to effectively eliminate noise while preserving diagnostic information, unlike earlier methods that relied on standard filters.

Segmentation: ROI extraction is performed using a threshold-based metaheuristic algorithm, Modified AOA, offering improved precision compared to conventional segmentation techniques.

Disease detection: A ViT is employed as the first-level classifier, diverging from the typical use of CNN or traditional ML models.

Plaque grading: A SVM serves as the second-level classifier, enabling quantification of plaque severity. To the best of the authors' knowledge, this is the first attempt to apply a two-level classification strategy for CCA diagnosis.

Another key contribution lies in integrating preprocessing, segmentation, and a two-level classification pipeline into a single framework, advancing the system toward real-time applicability. Additionally, this work employs the publicly available CUBS database, which has been annotated to provide a valuable benchmark for future research. The proposed CADS demonstrates superior performance in noise reduction, segmentation accuracy, and classification tasks. Unlike most prior studies that focus only on segmentation or disease detection, the system not only distinguishes normal and abnormal CCA images but also categorizes plaque type. By unifying all these components, the framework emerges as a distinct and comprehensive solution for CCA detection and grading.

The innovations and contributions of this work are as follows: Unlike earlier approaches, this paper proposes a fully automated pipeline for carotid artery disease diagnosis and plaque grading. A novel two-level classification strategy combining ViT and SVM is introduced. In this framework, ViT distinguishes normal from abnormal cases, while SVM grades plaque severity, a hierarchical structure not present in earlier approaches. This multistage design achieves higher accuracy than conventional single-level classifiers. A CMF is employed to effectively denoise images while preserving vessel structures, and a threshold-based segmentation using Modified AOA ensures precise ROI extraction, outperforming other methods. The framework is validated on the CUBS database, demonstrating improved scalability and robustness

compared to existing methods. To the best of the author's knowledge, this is the first fully automated CADS framework designed for both diagnosis and plaque grading in carotid artery disease.

3. PROPOSED METHODOLOGY

The potential of DL models to interpret and evaluate a significant number of medical images with high accuracy has attracted a significant amount of academic attention in recent years. In this paper, a complete automated system is proposed to diagnose CCA disease. Figure 1 shows an overview of the proposed CADS. The introduced system has five phases, namely noise filtering, segmentation, IMT measurement, classification, and plaque classification. The first phase involves eliminating noise from US images to improve image quality. The second phase focuses on isolating ROI from the filtered US image. In the third phase, some methods for processing images, such as edge detection, boundary extraction, and thresholding selection, are utilized to precisely extract the ROI. The next phase is dedicated to estimating IMT. The fourth phase categorizes US images into normal (no plaque) and abnormal (plaque present). Finally, the fifth phase quantifies the plaque in the abnormal US images. The designed system has been validated using US images from the CUBS database. Each phase of the system is elaborated as follows.

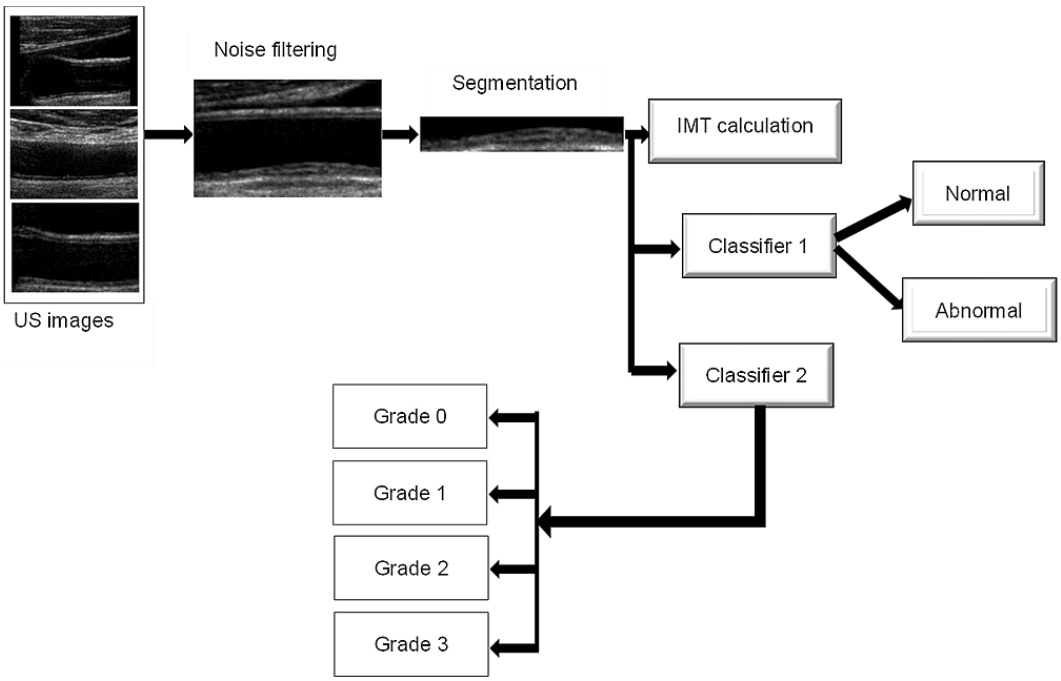

Figure 1. Pipeline of the proposed Computer-Aided Diagnosis System for Common Carotid Artery disease diagnosis

3.1 Noise suppression

Speckle noise is an inherent effect of image determination on US images. The noise present in the US image degrades image quality and reduces contrast. In this study, speckle noise in US images is reduced using the Circular Hybrid Median Filter (CMF). Median Filter (MF) is used owing to its power to eliminate speckle noise without losing significant information. With MF, a type of non-linear filter, the median of the nearby pixel values is used to replace each pixel value, maintaining edges and boundaries while removing noise [27]. These pixels are arranged using the CMF filter, which also substitutes the middle pixel value for the center pixel value.

Figure 2 shows an example of a preprocessed image. After denoising, the use of histogram equalization enhances the image's contrast. In the US image, each pixel has a certain intensity value that corresponds to the amplitude of the echoes returned from different tissues. These values are typically in the range between 0 and 255. First, the Cumulative Distribution Function (or CDF) is computed after computing the US image's histogram. The CDF is used to map each pixel in the US image to a new intensity value. The image's histogram is essentially uniform after this mapping redistributes pixel values. Histogram equalization improves the contrast and visibility of structures in the image, making it easier for automated systems to interpret the results.

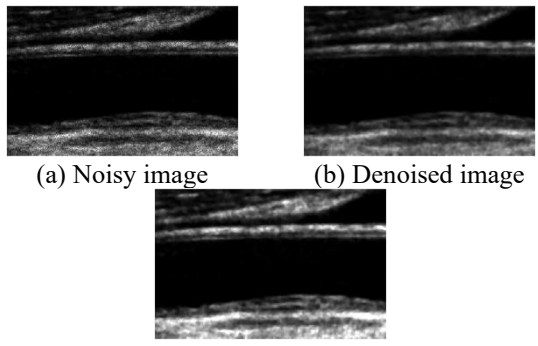

(a) Noisy image (b) Denoised image

(c) Image enhancement using histogram equalization

Figure 2. Result of noise suppression

3.2 ROI isolation

ROI is extracted from the preprocessed image using image processing techniques like morphological operations, edge detection, boundary extraction, and segmentation.

3.2.1 Morphological operations

Morphological operations play a vital role in image processing by refining various image features. They are useful for clearing small regions, smoothing the edges, filling gaps in images and properly preparing for subsequent analysis. In this task, a morphological closing function is applied to address the small opening in the image. The closing function merges small gaps and inconsistencies in one image. A disk-shaped structuring element with a radius of 2 pixels is used. This process involves applying a dilation operation multiple times, followed by a single erosion operation. This sequence of operations ensures that the small openings are effectively merged, resulting in a cleaner image. After image enhancement, the image is converted into a binary image, and then a morphological operation is applied. The method that a structural element, S, structures an image, A, may be represented as:

$$A.S = (\mathrm{A} \oplus S) \ominus S \tag{1}$$

where, $\mathrm{A} \oplus S$ -dilation of the image and $(\mathrm{A} \oplus S) \ominus S$ - erosion. Binary image and morphological operation output are shown in Figure 3(a) and Figure 3(b), respectively.

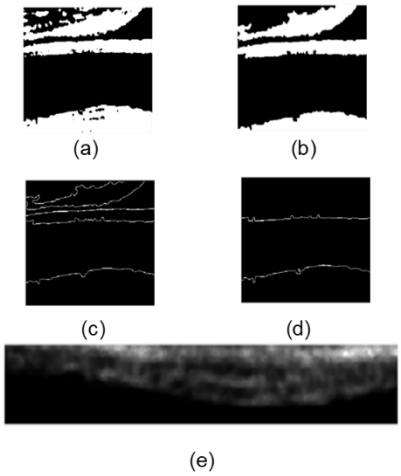

Figure 3. Segmentation outcome (a) Binary image, (b) morphology operation output, (c) Edge detection, (d) Far and near wall extraction, (e) Extracted ROI

3.2.2 Edge detection

Gaussian convolution is used to smooth the images before the Canny edge detector detects edges. The artery's actual edge is accurately shown by this process, which also helps to prevent noise from producing false lines. The tracked intensity discontinuity output image is produced by the effective edge detector after it receives input grayscale images. The canny operator is used to identify edges, as shown in Figure 3(c).

3.2.3 Extraction of boundary

It can select a random lumen point using the shortest column spanning index sum to identify the near-wall and far-wall borders. Until the gray value is found, the random point moves up and down. Based on region attributes, this value is used to derive the near-wall and far-wall boundaries.

3.2.4 Detection of the far wall

The IMT is measured at the far wall rather than the near wall for more accuracy, so it is calculated in the far wall area of a carotid US image. A region spanning 30 pixels upward and downward is removed once the random point has been found on the far-wall line. The extracted boundaries are displayed in Figure 3(d).

3.2.5 Segmentation based on optimized threshold

An effective technique for distinguishing between foreground and background images is the threshold-based image segmentation approach. There are a variety of optimization strategies that increase the challenge of identifying the optimum threshold values and their computational efficiency. Modified AOA is the most popular optimization algorithm in the system since it outperforms the existing optimization methods. In this study, multilevel thresholding is used for segmentation that utilizes interclass variance to identify the optimal threshold. The proposed system uses Modified AOA to isolate ROI with the objective function of Otsu's. Otsu's objective function is chosen owing to its ability to take less time compared to other thresholding techniques. The ROI is subjected to the threshold-based segmentation. Different thresholds are used to segment the carotid US images. Finding the threshold value is a comprehensive challenge, however. Each threshold value had to have its Otsu's function compared, and it was necessary to consider the threshold that produced the greatest objective function value as the optimum threshold. As all numbers from 0 to 255 have to be computed, it is computationally inefficient. Multilevel thresholding using Modified AOA and Otsu's objective function is used for segmentation to estimate IMT to address this problem. It is possible to express the objective function as:

$$OTh\ (t) = \sum_{j=1}^{N-1} \sigma_j \tag{2}$$

$$\sigma_i = \omega_i \left(m_i - m_\gamma\right)^2 \tag{3}$$

$$\omega_i = \sum_{i=j}^{t_{j+1}} (p_i) \tag{4}$$

$$m_i = \sum_{j=t_j}^{t_{j+1}} \frac{ip(i)}{\omega_i} \tag{5}$$

$$m_\gamma = \sum_{j=0}^{L-1} ip(i) \tag{6}$$

where, N-Number of thresholds, σ_i -Multi-class variance, ω_i-Probability of pixels in multi-class, t_j-Threshold, m_γ-Mean intensity of the image, m_i-Mean intensity of the i^{th} class.

The optimal threshold values are those values of t_j that maximize Oth(t). To increase the computational efficiency of determining the optimal threshold values, a variety of optimization strategies are available. This research uses the AOA out of all optimization methods since it produced superior results to the others.

According to Abualigah et al. [28], AOA is a novel kind of population-based algorithm. This optimization technique employs addition, subtraction, multiplication, and division. The key strength of AOA lies in its ability to solve optimization problems without the need for derivative calculations, which makes it versatile across different domains. AOA has been adopted to solve many problems like Alzheimer's disease, layout optimization, and plate structure classification. Despite its advantages, AOA faces difficulties like slow conversion and local optima. Therefore, this paper proposes the inclusion of inertia with a dynamic coefficient to

increase AOA's conversion speed and to prevent local optima. The results showed that the MAO has achieved better conversion speed and stability in the threshold optimization function.

(1) Standard AOA

In the standard AOA, addition and subtraction are used for exploitation, while multiplication and division facilitate exploration. By selecting a random integer r between 0 and 1, the Math Optimizer Accelerated (MOA) function establishes the search phase. Global exploration occurs if r > MOA(t); otherwise, local exploitation occurs. The definition of the MOA function is:

$$MOA(t) = min. + t \times \frac{(max. - min.)}{T} \tag{7}$$

where, t-Current iteration, T-Maximum iteration, min.-Minimum value and, max.-Maximum value.

(2) Exploration

During the exploration phase, AOA employs division and multiplication strategies to find better candidate solutions. It selects a random integer r1 [0,1]. One uses the division search technique if r1 < 0.5, and the multiplication search approach otherwise. The exploration process can be described as follows:

$$x(t+1) = \begin{cases} best(x) \div (MOP(t) + \varepsilon) \times B, & r1 < 0.5 \\ best(x) \times MOP(t) \times B, & otherwise \end{cases} \tag{8}$$

$$MOP(t) = 1 - t^{1/\propto} / T^{1/\propto} \tag{9}$$

$$B = (UB - LB) \times \mu + LB \tag{10}$$

where, X(t+1)-position at t+1 iteration; best(x)- position of the most competent individual from the various options; ε – a small number avoiding denominator from being 0; $\propto$ - sensitivity parameter; UB-upper boundary; LB-lower boundary; μ - parameter for the search process's control, which is set to 0.5 by experimentation; MOP-Math Optimizer Probability

(3) Exploitation

In the exploitation phase, AOA uses subtractive and additive search strategies. If random number r2 < 0.5, whenever possible, a subtractive search method is used; when not, an additive one. The exploitation process can be represented as:

$$x(t+1) = \begin{cases} best(x) - MOP(t) \times B, & r2 < 0.5 \\ best(x) + MOP(t) \times B, otherwise \end{cases} \tag{11}$$

(4) Proposed Modified AOA

Inertia weights are crucial for metaheuristic algorithms. Exploration benefits from larger inertia weights, while exploitation benefits from reduced inertia weights. The study improves the search efficiency of AOA by introducing an inertia weight that decreases exponentially and nonlinearly with the number of repetitions. Dynamic coefficients are also integrated to accelerate convergence and reduce local optima. The inertia weight can be represented as:

$$w(t) = k * w_{min} \left(\frac{w_{min}}{w_{max}}\right)^{1/(1+t/T)} \tag{12}$$

where, w_{min}-minimum inertia weight, w_{max}-maximum inertia weight, k-random value that changes dynamically around 1.

The Eqs. (8) and (11) can be rewritten as,

$$x(t+1) = \begin{cases} w(t) * best(x) \div (MOP(t) + \varepsilon) \times B, & r1 < 0.5 \\ w(t) * best(x) \times MOP(t) \times B, & otherwise \end{cases} \tag{13}$$

$$x(t+1) = \begin{cases} w(t) * best(x) - MOP(t) \times B, & r2 < 0.5 \\ w(t) * best(x) + MOP(t) \times B, otherwise \end{cases} \tag{14}$$

The extracted ROI is shown in Figure 3(e). The flowchart and Pseudo-code of the proposed Modified AOA are given in Figure 4 and Algorithm 1.

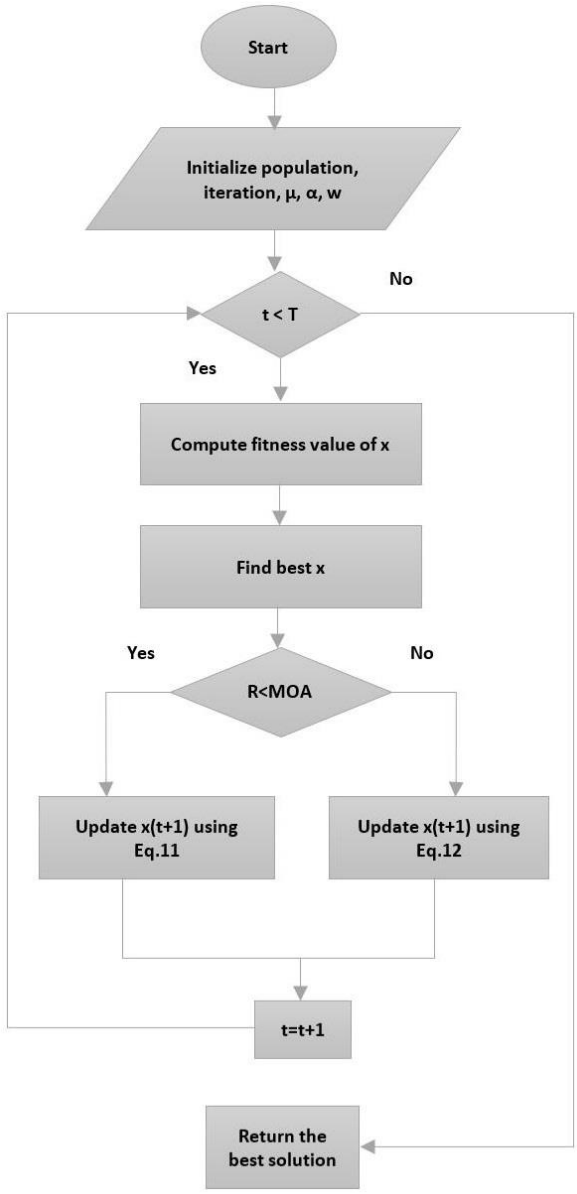

Figure 4. Flowchart of the proposed Modified Arithmetic Optimization Algorithm

Algorithm 1. Pseudo-code of the proposed Modified AOA

Initialize population size, M, dimension D, maximum number of iterations T, t=0, α, μ
Initialize the position of individual xi (i=1,2…M)
While (t<T)

update inertia weight using Eq. (11)
update MOA using Eq. (6)
update MOP using Eq. (8)
Compute the fitness function and find out best solution
For i=1,2…M do
For j=1=1,2,…D
Generate random numbers r, r1, r3 [0,1].
If r1 > MOA
update the position using Eq. (12)
else
update the position using Eq. (13)
end if
end for
end for
t=t+1
end while
Return the best solution

3.2.6 IMT calculation

Following the segmentation process, IMT is computed. There are the same number of sites on the identified LI and MA boundaries. Considering the identified LI and MA boundaries, the Mean Absolute Difference is provided by

$$IMT = \frac{1}{N}\sum_{r=1}^{N}|MA_r - LI_r| \quad (15)$$

where the LI and MA boundaries include n points. If the IMT value is less than 0.9, normal; else abnormal.

3.3 Classification of CCA

In this investigation, two classifiers are used to diagnose and quantify carotid disease. In the first-level classification, the purpose of a ViT is to classify CCA artery images as normal or abnormal. In the second level, an SVM is designed to grade the plaque in abnormal cases. As CNNs can extract deep features from input images during training, they are typically used for image classification tasks. Transformer-based models have performed effectively in Natural Language Processing (NLP) applications and computer vision tasks, including image categorization [29, 30]. CNN's restricted receptive fields make it difficult for them to represent the global context, even if they are excellent at extracting local data. In contrast, transformers can easily model the global context and have become widely used in computer vision. For this reason, the proposed CADS uses ViT for image classification. A detailed architecture of the proposed ViT is displayed in Figure 5. A grid of n x n patches is generated from the supplied image. Pixel values are combined to flatten each patch into a 1D vector. These vectors are linearly projected into a lower-dimensional space to form patch embeddings. These embeddings represent the input tokens for the transformer model. The transformer model introduces positional embeddings to the patch embeddings since it does not inherently understand the spatial structure of the image. The position of each patch in the original image is encoded by these positional embeddings, allowing the model to maintain an understanding of the spatial relationship between patches. The batch embeddings and positional information are passed via a series of transformer encoder layers. Multi-head feed-forward networks and self-attention techniques constitute each transformer encoder layer. The model also learns global connections between patches and concentrates on various portions of the image simultaneously because of the self-attention process.

The output corresponding to the token is sent into a classification head to produce the final class label after it has passed through the transformer encoder. As the objective function, the proposed ViT is trained by cross-entropy loss. The binary cross-entropy loss function is represented as follows:

$$L = -\frac{1}{n}\sum_{i=1}^{n}[y_i log(p_i) + (1 - y_i) log(1 - p_i)] \quad (16)$$

where, y_i – True label for sample, pi- For sample i, the expected probability of the positive class, n-total number of samples.

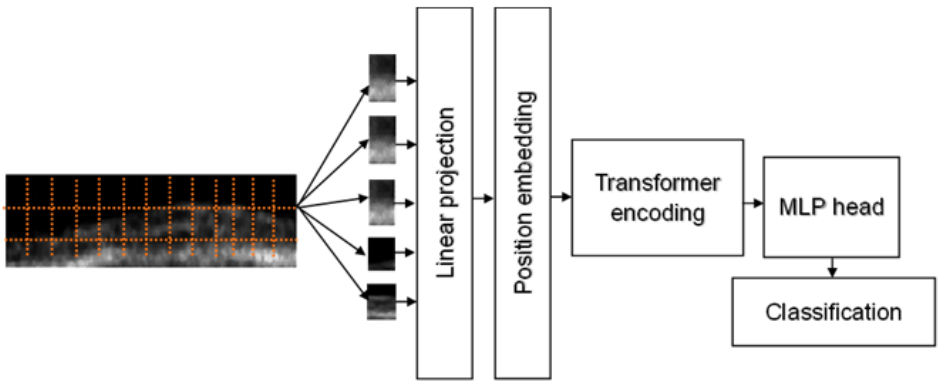

Figure 5. Structure of the proposed Vision Transformer

After the first level classification, SVM is employed to grade the plaque category. SVM is a popular supervised learning method for both regression and classification applications. SVMs are renowned for their ability to determine a margin of separation between classes and are especially useful for high-dimensional data. SVM is used with a radial basis function kernel and trained based on classification accuracy as a fitness function. The framework employs ViT for feature extraction due to its effectiveness in capturing global dependencies in image data, followed by an SVM for grading tasks, taking advantage of its robustness in high-dimensional feature spaces and suitability for CCA images. This combination was selected to balance the representation power of DL with the generalization ability and computational

efficiency of traditional ML. Multitask DL approaches are not adopted in this study because they generally require complex optimization, which may lead to overfitting.

4. EXPERIMENTAL RESULTS AND DISCUSSION

4.1 Details of the data set

The proposed CADS system was designed and tested using MATLAB 2022a running on an Intel Core i5 CPU @ 2.73 GHZ processor with 16GB RAM. Performance of the proposed CADS was tested on the CUBS database [31]. The database consisted of 2176 images, which included both normal and abnormal images. A broadband L12-5 MHz linear array transducer was used with a Philips (ATL) HDI 5000 duplex scanner for all scans. For every topic, numerous images were taken, and the operator who captured the image selected the finest ones.

All acquisitions used the same set of US characteristics, such as high frame rate and low persistence. A trained operator used a MyLab25 equipment with a LA523 4-13 MHz linear array transducer to acquire all scans. It used both digital and manual measuring techniques for all 2175 images. From this database, a total of 950 CCA images, which include 455 normal images and 495 abnormal images were chosen for validation. The effectiveness of the proposed CADS system was assessed by a 10-fold cross-validation method.

4.2 Evaluation metrics

Peak-Signal-to-Noise Ratio (PSNR) and Correlation Coefficient (CC), which measure how comparable noisy and denoised images are, have been used to assess the denoising performance of the suggested CMF.

$$PSNR = 10.log_{10}\left(\frac{max^2}{MSE}\right) \tag{17}$$

$$\text{MSE} = \frac{1}{MXN}\sum_{i=1}^{M}\sum_{j=1}^{N}[I(i,j) - K(i,j)]^2 \tag{18}$$

$$\text{NCC} = \frac{\sum_{i=1}^{M}\sum_{j=1}^{N}[I(i,j) - \bar{I}]\,[K(i,j) - \bar{K}]}{\sqrt{\sum_{i=1}^{M}\sum_{j=1}^{N}[I(i,j) - \bar{I}]^2 \sum_{i=1}^{M}\sum_{j=1}^{N}[K(i,j) - \bar{K}]^2}} \tag{19}$$

The degree of similarity between the suggested approaches and the ground truth has been measured using the Jaccard Similarity Coefficient (JSC) and Dice Coefficient (DC) to evaluate the ROI segmentation performance [32]:

$$\text{JSC(P, Q)} = \frac{|P \cap Q|}{|P \cup Q|} \tag{20}$$

$$\text{DC(P, Q)} = \frac{2|P \cap Q|}{|P| + |Q|} \tag{21}$$

Matthew's Correlation Coefficient (MCC), Balanced Accuracy (BA), Negative Predictive Value (NPV), F1-score, sensitivity, specificity, accuracy, and precision have all been used to assess the classification performance.

$$\text{Accuracy} = \frac{\text{TP} + \text{TN}}{\text{TP} + \text{TN} + \text{FP} + \text{FN}} \tag{22}$$

$$\text{Sensitivity/Recall} = \frac{\text{TP}}{\text{TP} + \text{FN}} \tag{23}$$

$$\text{Specificity} = \frac{\text{TN}}{\text{TN} + \text{FP}} \tag{24}$$

$$\text{BA} = \frac{Sensitivity + Specificity}{2} \tag{25}$$

$$\text{MCC} = \frac{\text{TPXTN} - \text{FPXFN}}{\sqrt{(\text{TP} + \text{FP})(\text{TP} + \text{FN})(\text{TN} + \text{FP})(\text{TN} + \text{FN})}} \tag{26}$$

$$\text{Precision} = \frac{\text{TP}}{\text{TP} + \text{FP}} \tag{27}$$

$$\text{F1 score} = 2 \times \frac{\text{Precision} \times \text{Recall}}{\text{Precision} + \text{Recall}} \tag{28}$$

$$\text{Specificity} = \frac{\text{TN}}{\text{TN} + \text{FN}} \tag{29}$$

where, TP- True Positive, TN- True Negative, FP- False Positive, and FN- False Negative.

4.3 Simulation results

4.3.1 Denoising performance analysis

In this work, CMF with a radius of 7 was employed to remove noise from the US images. Effectiveness of the CMF was assessed and compared with three different types of filters such as MF with a kernel size of 3 × 3, Weiner Filter (WF) with a kernel size of 3 × 3, and Gaussian Filter (GF). Quantitative analysis of these filters is reflected in Table 1. This analysis is based on two metrics: PSNR and NCC. As observed in Table 1, the CMF demonstrated the best performance with the highest PSNR and NCC, indicating it is highly effective in preserving both the quality and the structural details of the medical images. This superior performance of the CMF was attributed to its ability to use a circular neighborhood for median calculation, which is particularly beneficial in handling complex structures in the medical images without introducing artifacts. The MF filter operated on a 3x3 square neighborhood, did not capture the spatial variations as effectively as the CMF. This limitation resulted in lower PSNR and NCC values. While MF was good at noise reduction, it neither did nor preserved details as well.

Table 1. Performance comparison of various denoising filters

Metrics	CMF	Median Filter	Weiner Filter	Gaussian Filter
PSNR (dB)	33.47	28.75	26.24	27.12
NCC	0.986	0.902	0.814	0.899

The GF applied a weighted average based on a Gaussian distribution, which provided moderate performance. The output was blurred, leading to lower PSNR and MCC. This blurring effect contributed to the loss of critical details in medical images. The WF reduced noise based on local statistics. It showed the least performance with the lowest PSNR and NCC. Unlike MF, which used a square-shaped neighborhood, the CMF used a circular neighborhood. This shape was more natural and better aligned with the way features are distributed in images.

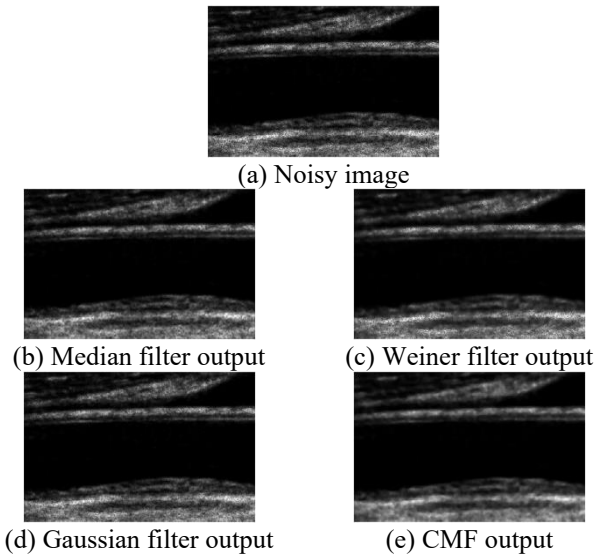

(a) Noisy image

(b) Median filter output (c) Weiner filter output

(d) Gaussian filter output (e) CMF output

Figure 6. Visual analysis of various denoising filters

The use of a larger radius allowed the CMF to consider a broader range of pixel values, making it more robust against high levels of noise while still preserving important features. This combination of a circular neighborhood and a larger radius enabled the CMF to outperform other filters, making it an ideal choice for the denoising of US medical images. Qualitative analysis of these filter outcomes is shown in Figure 6. The CMF processed images retained more of the original texture and structural details, while the images processed by MF, GF, and WF exhibited varying degrees of blurring and detail loss.

4.3.2 Segmentation performance analysis

After denoising, the proposed segmentation algorithm has been applied including edge detection, morphological operation, and Modified AOA optimized thresholding for isolating the affected region from its background. In Modified AOA, $\propto$ regulates the rate of transition from exploration to exploitation. A higher $\propto$ slows down exploitation, whereas a lower $\propto$ accelerates convergence but may risk premature local optimal. After testing, $\propto$ was set to 0.5, which provided an optimal trade-off between convergence and segmentation accuracy. The parameter k adjusts the inertia weight, which controls the step size during exploitation. A larger k increases exploration in early iterations, while a smaller k promotes fine-tuning in later iterations. The value of k was set to 0.8, which improved stability and prevented premature convergence. To validate these choices, a sensitivity analysis was conducted by varying $\propto$ and k across different ranges. Table 2 shows the performance, and the analysis shows that $\propto$ = 0.5 and k=0.8 yielded the best balance between segmentation accuracy and efficiency.

Table 2. Sensitivity analysis

$\propto$	k	Dice	Jaccard
0.1	0.2	0.842	0.727
0.1	0.5	0.86	0.754
0.1	0.8	0.842	0.727
0.3	0.2	0.882	0.789
0.3	0.5	0.9	0.818
0.3	0.8	0.882	0.789
0.5	0.2	0.895	0.810
0.5	0.5	0.899	0.817
0.5	0.8	0.911	0.837
0.7	0.2	0.882	0.789
0.7	0.5	0.9	0.818
0.7	0.8	0.882	0.789
0.9	0.2	0.842	0.727
0.9	0.5	0.86	0.754
0.9	0.8	0.842	0.727

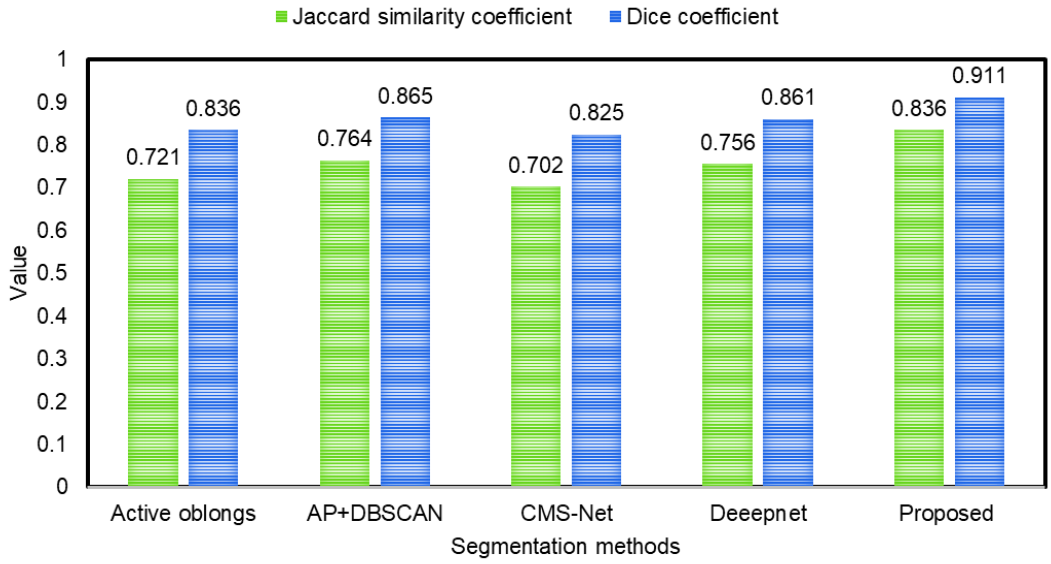

Figure 7. Comparative analysis of various segmentation algorithms

To demonstrate how the proposed technique is superior, segmentation performance was computed and compared against some earlier methods reported in the literature. All the past approaches were evaluated using the same images to ensure a realistic comparison. Figure 7 shows the segmentation performance comparison with earlier approaches. It is quite clear from Figure 7 that the proposed methods attained the highest JSC value of 0.836 and DC value of 0.911, indicating the best overall segmentation accuracy and overlap with the ground truth. The proposed Modified

AOA optimized threshold incorporated an advanced optimization technique that significantly enhanced the segmentation accuracy. The combination of Affinity Propagation followed by Density Based Spatial Clustering of Application with Noise (AB+DBSCAN) provided better performance than other methods, however, lower than the proposed method.

Mohammed et al. [1] applied Deepnet to separate the ROI from its background. The net attained JSC of 0.756 and DC of 0.861. However, it might not be as optimized as the proposed Modified AOA method. Latha et al. [17] utilized the AB+DBSCAN method and reported JSC of 0.764 and DC of 0.865. Active oblongs were used for image segmentation by Dhupia et al. [33]. This method yielded JSC and DC of 0.721 and 0.836, respectively. The active oblongs model may struggle with highly complex images, which can affect segmentation accuracy. Yuan et al. [34] designed CMS-Net for lumen CCA segmentation. This net has the lowest JSC of 0.702 and DC of 0.825 among the compared methods. While CMS-Net might be effective and efficient in some scenarios, it could be less effective in handling variations in lumen shape, leading to lower performance compared to other sophisticated methods. From the analysis, it is evident that the proposed method outperformed all other methods due to its optimization process that enhances segmentation accuracy.

4.3.3 Classification performance analysis

The proposed CADS has utilized ViT to categorize the CCA US images into normal (no plaque) or abnormal (plaque). A 10-fold cross-validation strategy was employed to evaluate generalization and minimize the risk of overfitting. To ensure that each sample contributed to both training and validation across runs, nine folds were employed for training and one fold for validation in each iteration. Training accuracy and loss plots are shown in Figure 8. The graph demonstrates stable convergence with accuracy approaching 100% and loss decreases smoothly toward zero. The consistency of results across folds confirms robustness and indicates that the model generalizes well without significant overfitting. The categorization performance has been evaluated using a number of assessment parameters of the model and these results have been contrasted against earlier methods, including ResNet-50 [20], MobileNet [35], CNN [36], AlexNet [37], and UNet++ [38]. Table 3 presents a comparative analysis of the proposed method against these alternatives.

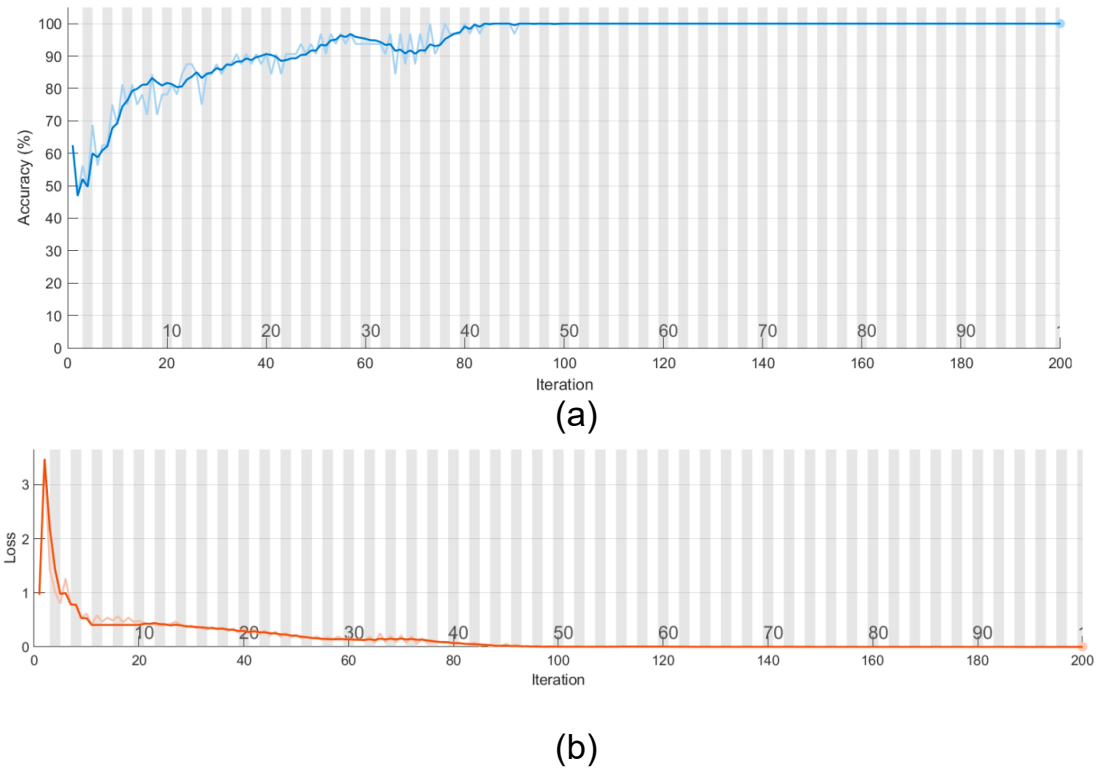

Figure 8. Training process (a) Training accuracy (b) Training loss

Table 3. Comparative analysis of different methods for Common Carotid Artery disease classification

Researchers	He et al. [20]	Chatterjee et al. [35]	Varma et al. [36]	Abd-Ellah et al. [37]	Li et al. [38]	Proposed
Models	ResNet 50	MobileNet	CNN	AlexNet	UNet++	ViT
Accuracy (%)	88.45	82.11	70.53	74.74	90.12	92.63
Specificity (%)	87.90	82.61	69.57	71.74	89.65	91.3
Sensitivity (%)	88.95	81.63	71.43	77.55	90.55	93.88
Precision (%)	89.1	83.33	71.43	74.51	90.25	92
NPV (%)	87.75	80.85	69.57	75	89.9	93.33
BA (%)	88.43	82.12	70.49	74.59	90.1	92.58
F1-score (%)	89.02	82.47	71.43	76	90.39	92.93
MCC	0.792	0.642	0.41	0.494	0.821	0.853

On observing classification accuracy, the proposed CADS achieved the highest accuracy, indicating its superior capability to correctly diagnose CCA. While MobileNet performed better than AlexNet and CNN, its classification accuracy was lower than that of the proposed CADS. The MobileNet, CNN, and AlexNet reported specificity values of 82.61%, 69.57%, and 71.74%, respectively. With the integration of more advanced architectures, ResNet-50 and UNet++ showed significant improvements across all metrics, achieving accuracies of 88.45% and 90.12%, respectively. However, the proposed model posed the highest specificity of 91.3%, indicating it is best at detecting TNs. Similarly, the proposed model excelled in recall, showing it accurately detected most of the positive cases. Precision was highest for the proposed model, indicating that it predicts most of the positive cases. Although AlexNet was also strong in this metric, it fell short compared to the CADS.

NPV value represents the ability of a classifier to correctly predict true negatives. The proposed CADS achieved the highest NPV, indicating it is very effective at predicting TNs. BA accounts for both sensitivity and specificity. The F1-score balances precision and sensitivity. The CADS gave the highest F1-score, indicating a well-balanced performance in precision and sensitivity. Moreover, the proposed CADS achieved the highest MCC, reflecting the quality of its classification. MCC value showed a strong correlation between predicted and actual classes. MobileNet exhibited moderate MCC, AlexNet and CNN had lower values.

Although MobileNet showed better accuracy and recall than AlexNet and CNN, it still produced more FPs compared to the CADS. Basic CNN can be easier to implement. This model yielded lower performance across all metrics compared to other models. Hence, less effective at diagnosing carotid artery disease. AlexNet performed better than CNN and offered reasonable accuracy, sensitivity, and precision. From the detailed analysis, it is evident that the proposed CADS demonstrated superior performance in diagnosing carotid artery disease compared to past methods.

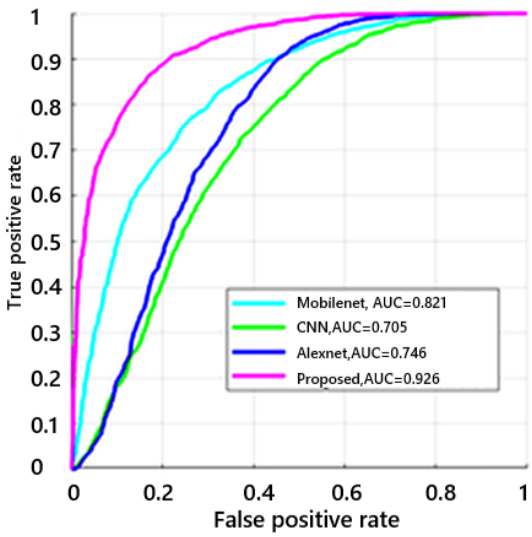

Figure 9. Receiver operating characteristic curve for common carotid artery diagnosis

A binary classifier system's ability to diagnose problems when its discriminating threshold changes is shown graphically by the Receiver operating characteristic (ROC) curve. The True Positive Rate (TPR) is plotted against the False Positive Rate (FPR) across multiple threshold values to get this curve. A model with an Area Under Curve (AUC) of 0 has no discrimination ability, while an AUC of 1 represents perfect discrimination. From Figure 9, it is observed that MobileNet [35] showed a good ability to distinguish between classes. The ROC curve for MobileNet showed that the TPR is significantly higher than the FPR across most threshold settings, indicating that it effectively identifies TP while minimizing FPs. The CNN [36] model showed moderate performance. While it achieved an acceptable ability to distinguish between classes, its performance was lower than that of MobileNet and CADS. AlexNet [37] demonstrated fair performance, slightly better than the CNN but still lower than CADS.

The proposed model exhibited an excellent performance, significantly surpassing all other models in its ability to distinguish between classes. The ROC curve for the proposed model indicates a much higher TPR relative to FPR across a broad range of thresholds, reflecting its superior capability in correctly classifying instances. This outstanding performance highlights the CADS's robustness and effectiveness as a classifier, making it the most reliable among the models evaluated.

4.3.4 Plaque grading performance analysis

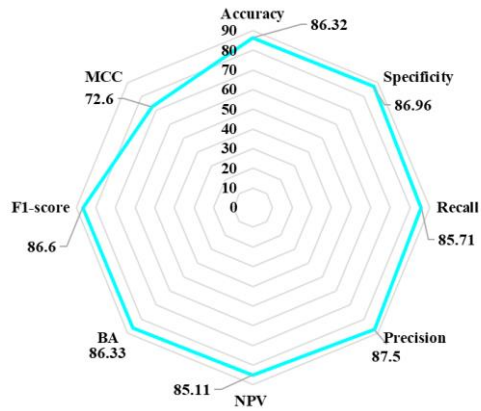

Figure 10. Plaque classification performance

The proposed system used SVM to grade the plaque in abnormal cases. The efficacy of the suggested CADS plaque grading is seen in Figure 10. The model gave an accuracy of 86.32% which means that the CADS correctly categorizes classes. The model was quite effective at correctly detecting negative cases with a specificity of 86.96%. An 85.71% recall showed the model was good at identifying positive cases. The model had a high probability of identifying positive cases are TP with a precision of 87.5%. An NPV of 85.11% indicates that most of the negative predictions are accurate. A BA of 86.33% indicated robust performance. F1-score of 86.6% reflected a good balance between precision and recall, representing the CADS's reliability in positive class prediction. An MCC of 72.6% represented overall good performance. The results proved that the model is well-suited for the task of plaque classification with high accuracy, balanced specificity and sensitivity, and strong overall reliability. ROC curve for plaque classification is depicted in Figure 11.

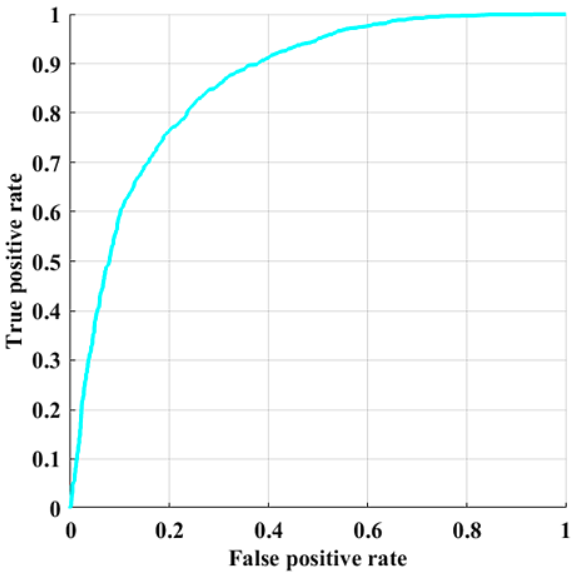

Figure 11. Receiver operating characteristic curve analysis for plaque grading

4.4 Discussion

In this paper, a CADS to diagnose CCA disease and grade plaque is proposed and implemented. The importance of this system lies in its potential to address carotid artery structure, which is characterized by carotid arterial narrowing. The disease is particularly insidious because it develops gradually over time, often starting in childhood and slowly progresses without noticeable symptoms. Preliminary identification is important to prevent the progression of atherosclerosis. By implementing this CAD, the purpose of this study is to provide a timely and accurate clinical tool that can significantly reduce the risk of stroke by detecting and classifying arterial plaque in its development.

The most significant contribution of this investigation is the introduction of a new framework that encompasses five distinct phases: denoising, lumen segmentation, classification of CCA as normal and abnormal, and further plaque classification. This structured approach not only enhances the accuracy of the CCA diagnosis but also addresses the gap in the literature, where a complete system for CCA diagnosis and plaque classification has yet to be fully proposed and reported. Each phase of the framework plays a vital role in ensuring that the CADS operates with high accuracy. For instance, the denoising phase is essential for improving the quality of the US images, thereby facilitating more accurate segmentation and classifications. The segmentation phase focuses on detecting the lumen, which is crucial for assessing the degree of narrowing. By incorporating these elements into a single system, this study pioneers a comprehensive solution to CCA diagnosis that is not only innovative but highly practical for clinical use.

A primary feature of CADS is the ability to combine multiple processes, including noise removal, segmentation and classification in the same structure. It addresses an important challenge in the integration field, where each of these processes is usually handled separately, often requiring different devices. By uniting these steps, the proposal system streamlines the clinical process, making it more efficient and less resource-intensive. The classification phase within this structure allows for the exclusion of normal images from the plaque classification process. This step is crucial as it reduces the computational load and speeds up the overall diagnosis, making the system more suitable for real-time deployment.

The comparative analysis in Table 3 clearly shows that the proposed CADS attained excellent performance across various metrics compared to other methods. The key observations are as follows:

- The proposed CADS achieved an accuracy of 92.63%, surpassing the Chatterjee et al. [35] method's accuracy of 82.11%, outperforming the Abd-Ellah et al. [37] method with 74.74% accuracy, and significantly exceeding the Varma et al. [36] method, which reported an accuracy of 70.53%. This significant improvement demonstrates the effectiveness with which the proposed CADS performs CCA image classification.
- The proposed CADS attained a specificity of 91.3%, significantly outperforming the specificity of 82.61% by Chatterjee et al. [35], 69.57% by Varma et al. [36] and 71.74% specificity by Abd-Ellah et al. [37]. This marked improvement underscores the performance of the CADS.
- The proposed CADS reported a sensitivity of 93.88%, surpassing the sensitivity of 81.63% attained by Chatterjee et al. [35], far exceeding the 71.43% sensitivity of Varma et al. [36] and outperforming the 77.55% reported by Abd-Ellah et al. [37].
- In terms of precision, the CADS reached 92%, a significant improvement over the 83.33% precision achieved by Chatterjee et al. [35], 71.43% by Varma et al. [36] and 74.51% reported by Abd-Ellah et al. [37]. This substantial gain highlights the robustness of CADS.
- Additionally, the proposed CADS recorded a BA of 92.58%, while Chatterjee et al. [35] reported 82.12%, Varma et al. [36] attained 70.49%, and Abd-Ellah et al. [37] achieved 74.59%.

The potential for real-time deployment of the CCA diagnosis system is one of the most significant advantages. Real-time processing is particularly valuable for radiologists, who require quick and accurate results to make informed decisions about patient care. By minimizing processing time, the system ensures that the diagnosis can be made promptly, which is essential in acute medical situations. The proposed model required approximately 53 seconds for training and 1.01 seconds for testing. These runtimes demonstrate that the model can be executed efficiently on standard hardware without the need for specialized computational resources. The outcomes indicate that the approach is computationally feasible for practical applications. The CADS system not only improves the speed and accuracy of the CCA diagnosis but also offers a scalable solution that can be adapted for use in a variety of clinical settings. As carotid artery disease remains a leading cause of stroke, the implementation of such advanced diagnostic tools is essential for improving patient outcomes and preventing severe complications associated with the disease.

The model was evaluated under standard experimental conditions without testing across varying noise levels, alternative data distributions, or imaging devices. Future studies will address this limitation by incorporating robustness experiments with noisy or low-quality images as well as validation on cross-device and multi-institutional datasets to ensure stability and broader applicability.

5. CONCLUSION AND RECOMMENDATIONS

In this paper, a novel automated system, CADS has been designed for CCA disease diagnosis. The proposed CADS involved many phases, such as preprocessing, segmentation, classification, and plaque classification. In the preprocessing phase, CMF was used to address speckle noise and improve the quality of the US images. The measured parameters such as PSNR and NCC showed better performance than other filters taken for comparison. In the segmentation phase, the Modified AOA optimized threshold was employed to separate the ROI from its background. In terms of quantitative assessment measures, the segmentation strategy that was proposed produced superior results. In the classification phase, ViT was employed to classify the images into normal and abnormal. Finally, SVM was utilized to categorize the images. Using the CUBS database, the suggested approach was evaluated. The model's efficacy was evaluated by a series of experiments. As a result of this investigation, the model achieved an impressive classification rate of 92.63% for disease diagnosis and 86.23% for plaque classification. Additionally, the performance of the model was compared with earlier approaches, demonstrating its superior performance in all aspects of CCA diagnosis. These results highlight the significance of advanced techniques employed for CCA diagnosis. The CADS model has the potential to assist physicians in diagnosing CCA more efficiently, reducing their workload and time.

In future research, hybrid metaheuristic algorithms, combining transformers with CNN-based models, will be implemented for improved model accuracy. Advanced feature selection methods will be explored to reduce feature dimensions to improve computation speed and reduce model complexity. The model will also be evaluated on datasets that include richer demographic and clinical metadata, which would allow for subgroup analysis and better assessment of model fairness and robustness. Additionally, incorporating data from multiple sources with diverse patient populations could help mitigate potential biases and improve the applicability of the proposed method in real-world scenarios. To ensure reliable performance and accuracy, the suggested system's performance will be assessed employing large and intricate datasets. To improve the system's adaptability, its effectiveness will be assessed using various imaging modalities, including CTA, PET, and MRI. Real-time implementation of the proposed CADS will be explored to ensure that it can operate efficiently in real-world clinical environments. Performance of the proposed system will be tested in real-world clinical environments to assess robustness and reliability.

REFERENCES

[1] Mohammed, H.H., Elharrouss, O., Ottakath, N., Al-Maadeed, S., Chowdhury, M.E., Bouridane, A., Zughaier, S.M. (2023). Ultrasound intima-media complex (IMC) segmentation using deep learning models. Applied Sciences, 13(8): 4821. https://doi.org/10.3390/app13084821

[2] World Health Organization. (2011). Global Atlas on Cardiovascular Disease Prevention and Control. https://www.who.int/cardiovascular_diseases/en/

[3] Menchón-Lara, R.M., Sancho-Gómez, J.L. (2015). Fully automatic segmentation of ultrasound common carotid artery images based on machine learning. Neurocomputing, 151: 161-167. https://doi.org/10.1016/j.neucom.2014.09.066

[4] Meshram, N.H., Mitchell, C.C., Wilbrand, S., Dempsey, R.J., Varghese, T. (2020). Deep learning for carotid plaque segmentation using a dilated U-Net architecture. Ultrasonic Imaging, 42(4-5): 221-230. https://doi.org/10.1177/0161734620951216

[5] Saxena, A., Ng, E.Y.K., Lim, S.T. (2019). Imaging modalities to diagnose carotid artery stenosis: Progress and prospect. Biomedical Engineering Online, 18(1): 66. https://doi.org/10.1186/s12938-019-0685-7

[6] Ottakath, N., Al-Maadeed, S., Zughaier, S.M., Elharrouss, O., Mohammed, H.H., Chowdhury, M.E., Bouridane, A. (2023). Ultrasound-based image analysis for predicting carotid artery stenosis risk: A comprehensive review of the problem, techniques, datasets, and future directions. Diagnostics, 13(15): 2614. https://doi.org/ 10.3390/diagnostics13152614

[7] Nagaraj, Y., Madipalli, P., Rajan, J., Kumar, P.K., Narasimhadhan, A.V. (2018). Segmentation of intima media complex from carotid ultrasound images using wind driven optimization technique. Biomedical Signal Processing and Control, 40: 462-472. https://doi.org/10.1016/j.bspc.2017.08.009

[8] Hossain, M.M., AlMuhanna, K., Zhao, L., Lal, B.K., Sikdar, S. (2015). Semiautomatic segmentation of atherosclerotic carotid artery wall volume using 3D ultrasound imaging. Medical Physics, 42(4): 2029-2043. https://doi.org/10.1118/1.4915925

[9] Xu, X., Zhou, Y., Cheng, X., Song, E., Li, G. (2012). Ultrasound intima–media segmentation using Hough transform and dual snake model. Computerized Medical Imaging and Graphics, 36(3): 248-258. https://doi.org/10.1016/j.compmedimag.2011.06.007

[10] Miceli, G., Rizzo, G., Basso, M.G., Cocciola, E., Pennacchio, A.R., Pintus, C., Tuttolomondo, A. (2023). Artificial intelligence in symptomatic carotid plaque detection: A narrative review. Applied Sciences, 13(7): 4321. https://doi.org/10.3390/ app13074321

[11] Maitra, M., Chatterjee, A. (2008). A hybrid cooperative–comprehensive learning based PSO algorithm for image segmentation using multilevel thresholding. Expert Systems with Applications, 34(2): 1341-1350. https://doi.org/10.1016/j.eswa.2007.01.002

[12] Tao, W., Jin, H., Liu, L. (2007). Object segmentation using ant colony optimization algorithm and fuzzy entropy. Pattern Recognition Letters, 28(7): 788-796. https://doi.org/10.1016/j.patrec.2006.11.007

[13] Bhandari, A.K., Singh, V.K., Kumar, A., Singh, G.K. (2014). Cuckoo search algorithm and wind driven optimization-based study of satellite image segmentation for multilevel thresholding using Kapur's entropy. Expert Systems with Applications, 41(7): 3538-3560. https://doi.org/10.1016/j.eswa.2013.10.059

[14] Rocha, R., Silva, J.A., Campilho, A.J. (2011). Dynamic programming and fuzzy classification for the automatic segmentation of the carotid in ultrasound images. In IAPR Conference on Machine Vision Applications, Nara, Japan, pp. 552-556

[15] Naik, V., Gamad, R.S., Bansod, P.P. (2013). Carotid artery segmentation in ultrasound images and measurement of intima-media thickness. BioMed

Research International, 2013(1): 801962. https://doi.org/10.1155/2013/801962
[16] Molinari, F., Raghavendra, U., Gudigar, A., Meiburger, K.M., Rajendra Acharya, U. (2018). An efficient data mining framework for the characterization of symptomatic and asymptomatic carotid plaque using bidimensional empirical mode decomposition technique. Medical & Biological Engineering & Computing, 56(9): 1579-1593. https://doi.org/10.1007/s11517-018-1792-5
[17] Latha, S., Samiappan, D., Muthu, P., Kumar, R. (2021). Fully automated integrated segmentation of carotid artery ultrasound images using DBSCAN and affinity propagation. Journal of Medical and Biological Engineering, 41(2): 260-271. https://doi.org/10.1007/s40846-020-00586-9
[18] Vila, D.M.M., Remeseiro, B., Grau, M., Elosua, R., Betriu, A., Fernandez-Giraldez, E., Igual, L. (2020). Semantic segmentation with DenseNets for carotid artery ultrasound plaque segmentation and CIMT estimation. Artificial Intelligence in Medicine, 103: 101784. https://doi.org/10.1016/j.artmed.2019.101784
[19] Huang, Q., Tian, H., Jia, L., Li, Z., Zhou, Z. (2023). A review of deep learning segmentation methods for carotid artery ultrasound images. Neurocomputing, 545: 126298. https://doi.org/10.1016/j.neucom.2023.126298
[20] He, L., Yang, Z., Wang, Y., Chen, W., Diao, L., Wang, Y., Shen, E. (2024). A deep learning algorithm to identify carotid plaques and assess their stability. Frontiers in Artificial Intelligence, 7: 1321884. https://doi.org/10.3389/frai.2024.1321884
[21] Kumar, J.H., Teotia, K., Raj, P.K., Andrade, J., Rajagopal, K.V., Seelamantula, C.S. (2019). Automatic segmentation of common carotid artery in longitudinal mode ultrasound images using active oblongs. In ICASSP 2019-2019 IEEE International Conference on Acoustics, Speech and Signal Processing (ICASSP), Brighton, UK, pp. 1353-1357. https://doi.org/10.1109/ICASSP.2019.8682301
[22] Jain, P.K., Sharma, N., Saba, L., Paraskevas, K.I., Kalra, M.K., Johri, A., Suri, J.S. (2021). Automated deep learning-based paradigm for high-risk plaque detection in B-mode common carotid ultrasound scans: An asymptomatic Japanese cohort study. International Angiology, 41: 9-23. https://doi.org/10.23736/S0392-9590.21.04771-4
[23] Özdemir, H.İ., Atman, K.G., Şirin, H., Çalık, A.E., Senturk, I., Bilge, M., Çınar, C. (2024). Super learner algorithm for carotid artery disease diagnosis: A machine learning approach leveraging craniocervical CT angiography. Tomography, 10(10): 1622-1644. https://doi.org/10.3390/ tomography10100120
[24] Fitas, R., Gonçalves, J. (2024). Improving computer-aided medical diagnosis using generative adversarial networks for carotid artery ultrasound image data augmentation and classification. Journal of Electrical Engineering and Computer (JEECOM), 6(1): 138-149. https://doi.org/10.33650/jeecom.v6i1.8006
[25] Koloi, A., Loukas, V.S., Hourican, C., Sakellarios, A.I., Quax, R., Mishra, P.P., Fotiadis, D.I. (2024). Predicting early-stage coronary artery disease using machine learning and routine clinical biomarkers improved by augmented virtual data. European Heart Journal-Digital Health, 5(5): 542-550. https://doi.org/10.1093/ehjdh/ztae049
[26] Ottakath, N., Akbari, Y., Al-Maadeed, S.A., Bouridane, A., Zughaier, S.M., Chowdhury, M.E. (2024). Bi-attention DoubleUNet: A deep learning approach for carotid artery segmentation in transverse view images for non-invasive stenosis diagnosis. Biomedical Signal Processing and Control, 94: 106350. https://doi.org/10.1016/j.bspc.2024.106350
[27] Gagan, J.H., Shirsat, H.S., Mathias, G.P., Mallya, B.V., Andrade, J., Rajagopal, K.V., Kumar, J.H. (2022). Automated segmentation of common carotid artery in ultrasound images. IEEE Access, 10: 58419-58430. https://doi.org/10.1109/ACCESS.2022.3179402
[28] Abualigah, L., Diabat, A., Mirjalili, S., Abd Elaziz, M., Gandomi, A.H. (2021). The arithmetic optimization algorithm. Computer Methods in Applied Mechanics and Engineering, 376: 113609. https://doi.org/10.1016/j.cma.2020.113609
[29] Dosovitskiy, A., Beyer, L., Kolesnikov, A., Weissenborn, D., Zhai, X., Unterthiner, T., Houlsby, N. (2020). An image is worth 16x16 words: Transformers for image recognition at scale. arXiv preprint arXiv:2010.11929. https://doi.org/10.48550/arXiv.2010.11929
[30] Hamano, G., Imaizumi, S., Kiya, H. (2022). Image classification using vision transformer for EtC images. In 2022 Asia-Pacific Signal and Information Processing Association Annual Summit and Conference (APSIPA ASC), Chiang Mai, Thailand, pp. 1506-1513. https://doi.org/10.23919/APSIPAASC55919.2022.9980144
[31] Meiburger, K.M., Zahnd, G., Faita, F., Loizou, C.P., Carvalho, C., Steinman, D.A., Molinari, F. (2021). Carotid ultrasound boundary study (CUBS): An open multicenter analysis of computerized intima–media thickness measurement systems and their clinical impact. Ultrasound in Medicine & Biology, 47(8): 2442-2455. https://doi.org/10.1016/j.ultrasmedbio.2021.03.022
[32] Kabir, S., Wagner, C., Havens, T.C., Anderson, D.T. (2020). A similarity measure based on bidirectional subsethood for intervals. IEEE Transactions on Fuzzy Systems, 28(11): 2890-2904. https://doi.org/10.1109/TFUZZ.2019.2945249
[33] Dhupia, A., Kumar, J.H., Andrade, J., Rajagopal, K.V. (2020). Automatic segmentation of lumen intima layer in longitudinal mode ultrasound images. In 2020 42nd Annual International Conference of the IEEE Engineering in Medicine & Biology Society (EMBC), Montreal, QC, Canada, pp. 2125-2128. https://doi.org/10.1109/EMBC44109.2020.9175831
[34] Yuan, Y., Li, C., Xu, L., Zhu, S., Hua, Y., Zhang, J. (2022). CSM-Net: Automatic joint segmentation of intima-media complex and lumen in carotid artery ultrasound images. Computers in Biology and Medicine, 150: 106119. https://doi.org/10.1016/j.compbiomed.2022.106119
[35] Chatterjee, A., Nair, J.R., Ghoshal, T., Latha, S., Samiappan, D. (2020). Diagnosis of atherosclerotic plaques in carotid artery using transfer learning. In 2020 5th International Conference on Communication and Electronics Systems (ICCES), Coimbatore, India, pp. 1247-1251. https://doi.org/10.1109/ICCES48766.2020.9138052
[36] Varma, S., Dhanalakshmi, S., Latha, S. (2020). Performance evaluation of unpreprocessed and pre-processed ultrasound images of carotid artery using CNN

algorithm. IOP Conference Series: Materials Science and Engineering, 912(2): 022030. https://doi.org/10.1088/1757-899X/912/2/022030

[37] Abd-Ellah, M.K., Khalaf, A.A., Gharieb, R.R., Hassanin, D.A. (2023). Automatic diagnosis of common carotid artery disease using different machine learning techniques. Journal of Ambient Intelligence and Humanized Computing, 14(1): 113-129. https://doi.org/10.1007/s12652-021-03295-6

[38] Li, H., Song, W., Liu, A., Qin, P. (2025). DBF-UNet: A two-stage framework for carotid artery segmentation with pseudo-label generation. arXiv preprint arXiv:2504.00908. https://doi.org/10.48550/arXiv.2504.00908